Electroporation-Induced Formation of Individual Calcium Entry Sites in the Cell Body and Processes of Adherent Cells

Mary N. Teruel and Tobias Meyer
Department of Cell Biology, Duke University Medical Center, Durham, North Carolina 27710 USA

ABSTRACT Electroporation is a widely used method for introducing macromolecules into cells. We developed an electroporation device that requires only 1 μl of sample to load adherent cells in a 10-mm^2 surface area while retaining greater than 90% cell survivability. To better understand this device, field-induced permeabilization of adherent rat basophilic leukemia and neocortical neuroblastoma cells was investigated by using fluorescent calcium and voltage indicators. Rectangular field pulses led to the formation of only a few calcium entry sites, preferentially in the hyperpolarized parts of the cell body and processes. Individual entry sites were formed at the same locations when field pulses were repeated. Before calcium entry, a partial breakdown of the membrane potential was observed in both polar regions. Based on our results, a model is proposed for the formation and closure of macromolecule entry sites in adherent cells. First, the rapid formation of a large number of small pores leads to a partial membrane potential breakdown in both polar regions of the cell. Second, over tens of milliseconds, a few entry sites for macromolecules are formed, preferentially in the hyperpolarized part of cell body and processes, at locations defined by the local membrane structure. These entry sites reseal on a time scale of 50 ms to several seconds, with residual small pores remaining open for several minutes.

INTRODUCTION

Transient permeabilization of the plasma membrane occurs when electric fields are applied above a critical breakdown voltage (Kinosita and Tsong, 1977a). This process was termed electroporation and has been exploited for the transfection of cells with cDNA and for the introduction of other membrane impermeant molecules into the cytosol (for reviews, see Chang et al., 1992; Tsong, 1991; Zhelev and Needham, 1994; Sowers, 1995). In most practical applications, cells are electroporated in suspension. Before application of an electric field pulse, the cDNA or other sample is mixed together with the cells in a cuvette, typically 100 μl to 1 ml in volume. There has been much interest in developing adherent cell electroporation techniques in order to avoid removing cultured cells from their substratum and introducing unwanted physiological effects (Yang et al., 1995; Raptis et al., 1995; Zheng and Chang, 1991; Maurel et al., 1989). Moreover, electroporating cells in their attached state rather than in suspension has been shown to yield a higher transfection rate (Zheng and Chang, 1991). In applications of adherent cell electroporation techniques, epithelial cells were electroporated with heparin for subsequent investigations of calcium signaling by fluorescence microscopy of calcium indicators (Boitano et al., 1992), and Lucifer yellow was used to examine intercellular gap junctional communication (Raptis et al., 1995). Teissie et al. (1982) have also shown that electropulsation of adherent cells can also be used for electrofusion.

Received for publication 6 January 1997 and in final form 23 June 1997.
Address reprint requests to Dr. Tobias Meyer, Department of Cell Biology, Nanaline Duke Bldg., Rm. 346, Box 3709, Duke University Medical Center, Durham, NC 27710. Tel.: 919-681-8072; Fax: 919-681-7978; E-mail: tobias@cellbio.duke.edu.

0006-3495/97/10/1785/12 $2.00

Our interest in the mechanism of pore formation in adherent cells came from our experimental need to load cells with photoreleasable inositol 1,4,5-trisphosphate and membrane-impermeable calcium indicators (Oancea and Meyer, 1996), as well as to introduce in vitro transcribed mRNA into cultured mammalian cells (Yokoe and Meyer, 1996). In contrast to DNA transfection, in vivo protein synthesis from electroporated RNA can be used in all cell types and enables researchers to conduct studies with the expressed proteins as soon as 2 h after electroporation. Another advantage of using RNA instead of DNA is that functional measurements in cells can be made in the presence of the expressed protein, and control measurements can be performed before RNA electroporation and after the degradation of RNA and protein. However, using currently available suspension or adherent cell electroporation methods would have been prohibitively expensive because large amounts of costly sample (i.e., mRNA, peptides, or photoreleasable bioactive compounds) are required to be mixed with the electroporation media. To carry out our studies, we developed a device that requires only 1 μl of sample to electroporate adherent cells in a 10-mm^2 area. We have continued to improve this method of small volume electroporation and have obtained an efficient and easy-to-use device, or "microporator," which is also described here. References to other small-volume electroporation devices are included in the Materials and Methods section.

Significant inroads into the understanding of electric field-induced permeabilization of lipid bilayers and biological membranes have been made in the past, and many parameters have been explored for optimal permeabilization, such as field pulse length and duration, as well as different pulse shapes (for reviews see Chang et al., 1992; Shigekawa and Dower, 1988; Hui, 1995). However, many of the earlier studies were performed with field pulses

shorter than 1 ms, and now it appears that better electroporation of mammalian cells is achieved with longer field pulses above 10 ms (for example, Baum et al., 1994; EC100 Electroporator manual, E-C Apparatus Corp., St. Petersburg, FL; BioRad GenePulser manual, Biorad Laboratories, Richmond, CA). In addition, most earlier studies were performed on artificial bilayers or round cells and not with adherent cells, which often have complex morphologies with filopodias, neurites, or other cell processes. In the present study, we investigated field-induced pore formation by using the same rectangular field stimulation protocols that lead to the efficient loading of adherent mammalian cells with RNA and other large molecules (see also Yokoe and Meyer, 1996). We report that such long rectangular field pulses, which result in more than 90% cell viability, induce only a few large calcium entry sites. These calcium entry sites are located preferentially in the hyperpolarized regions of cell body and processes, and individual entry sites are formed at the same locations in response to repetitive field pulses.

MATERIALS AND METHODS

Cell cultures

This study investigated calcium entry site formation in two types of cells, rat basophilic leukemia cells (2H3 type, a tumor mast cell line) and neocortical neuroblastoma cells (Chun and Jaenisch, 1996). RBL cells were grown at 37°C and 5% CO_2 in Dulbecco's minimum essential medium (DMEM) with 20% fetal bovine serum (Gibco BRL), 4 mM L-glutamine, and 10 μg/ml Gentamicin Reagent Solution (Gibco BRL). RBL cells were plated directly on glass coverslips at least 2 h before each experiment. The neocortical neuroblastoma cells were grown at 37°C and 5% CO_2 in Opti-MEM I containing 2.5% heat-inactivated fetal calf serum (ifcs) (Hyclone), 20 mM D-glucose, 55 μM β-mercaptoethanol, 1% v/v penicillin (5000 U/ml), and streptomycin (5000 μg/ml). The same medium was used for plating the cells, except that the percentage of ifcs was reduced from 2.5% to 2%. Reducing the amount of ifcs "starved" the cells and tended to result in more elongated cells with more neurites (recommendation from Dr. J. Chun, UCSD, San Diego, CA). Cells were plated on glass coverslips coated with Cell-Tak (Collaborative Biomedical, Bedford, MA) at least 8 h before each experiment.

During experiments, the culturing medium of the RBL cells and neuroblastoma cells was replaced with an extracellular buffer consisting of 135 mM NaCl, 5 mM KCl, 20 mM HEPES (pH 7.4), 1.5 mM $CaCl_2$, 1.5 mM $MgCl_2$, and 10 mM glucose. When experiments with the calcium indicator fluo-3 AM (Molecular Probes, Eugene, OR) were carried out, 250 μM sulfinpyrazone (Sigma) was added to the extracellular buffer to prevent the indicator from being transported out of the cells. Fluo-3 AM was loaded by incubating the cells for at least 30 min in a solution consisting of 2 μM fluo-3 AM and 250 μM sulfinpyrazone in extracellular buffer. The solution used to load the cells with the voltage-sensitive indicator di-8-ANEPPS (Molecular Probes) consisted of 15 μM di-8-ANEPPS in extracellular buffer. The cells were incubated with the di-8-anepps solution for 15 min at 4°C (the low temperature was needed to minimize endocytosis). Before electroporation, coverslips were taken out of the petri dishes, and a Teflon ring was sealed onto each coverslip with vacuum grease. The resulting dish formed by the ring and the coverslip could hold up to 1.1 ml of liquid. Cells were then washed three times with the extracellular buffer. The extracellular buffer was also used as the electroporation medium. The intracellular buffer used in some experiments consisted of 135 mM KCl, 5 mM NaCl, 1.5 mM $CaCl_2$, 20 mM HEPES (pH 7.4), 1.5 mM $MgCl_2$, and 10 mM glucose. All experiments were carried out at room temperature (~25°C).

Small-volume electroporation device for adherent cells

A self-built electroporation device was used for cell loading. Examples of electroporation devices that use small sample volumes have been described earlier for cells in suspension (Kinosita and Tsong, 1979; Sowers, 1984; Hibino et al., 1991). Zheng and Chang (1991) have built an electroporation device with two wire electrodes that can be used to electroporate adherent cells in a small surface area. As discussed in the Introduction, using small sample volumes reduces the cost of experiments, and adherent cells are often desirable for experimental protocols. Therefore, in our electroporation device we have combined the advantages of small sample volumes with those of using adherent cells for electroporation. With this efficient and easy-to-use device, the average time to position, inject sample onto, and electroporate cells plated on a surface is ~1 min. Thus series of experiments can be quickly performed.

The main new feature of this device is a foot structure that can be rapidly lowered onto cells cultured on ordinary coverslips or other flat substrates (Fig. 1 *A*). The actual electroporated volume is limited by a 100-μm-deep rectangular rim around the edge of the bottom of the foot (Fig. 1 *B*). This rim is critical in reducing the sample volume between the bottom of the foot and the cells on the coverslip into the range of

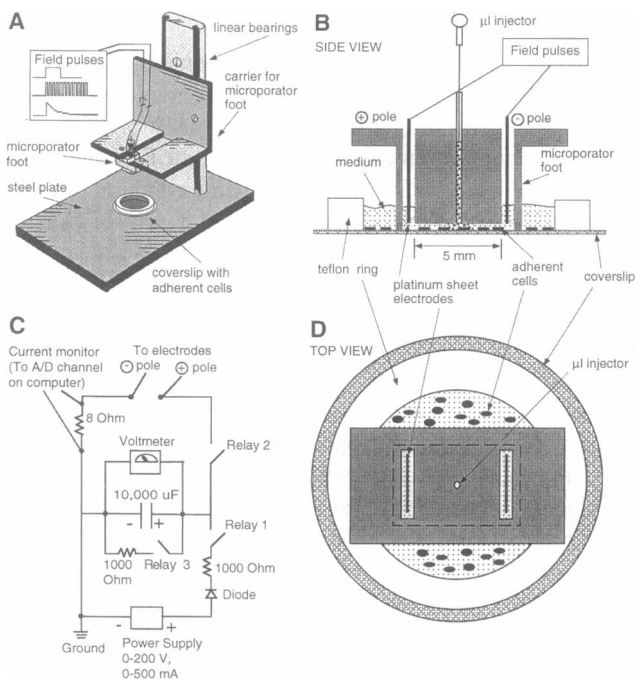

FIGURE 1 Diagram of a microporator apparatus used for electroporation of adherent cells. (*A*) View of the overall design of the microporator. The actual microporator foot is mounted on a carrier that can be lowered onto the coverslip with linear bearings. Different field pulse generators can readily be connected to the apparatus. The adherent cells are plated on coverslips, and the medium is kept on top of the cells by a Teflon ring. (*B*) Cross section through the actual microporator foot. The space between the bottom of the foot and the coverslip is confined by a 100-μm-thick rim that surrounds the foot. The actual electroporated area is a 5 × 5 mm region with two platinum electrodes placed on two of its sides. The O_2 and H_2 generated at the respective electrodes during electroporation can exit the poration area through slits drilled into the foot structure. A microliter injector consisting of a Teflon tube with a wire plunger is used to apply a sample volume of 0.5–2 μl. (*C*) Schematic representation of the electronics used to pulse the microporator foot, as well as the wire electrodes used in the rapid confocal imaging experiments. (*D*) Top view of the microporator foot.

microliters. The device uses sample volumes of 0.5–2 μl to electroporate cells in an area of 5–20 mm^2. Two platinum sheet electrodes are fixed in the foot structure and hang down to define a 5 mm × 5 mm electroporation area (Fig. 1, *B* and *D*). The O_2 and H_2 generated at the respective electrodes during electroporation can exit the poration area through slits drilled into the foot structure. The sample is applied directly into the center of the electroporation area with a microliter injector consisting of a Teflon tube with a wire plunger.

For most applications, the medium above the cells on the coverslip is contained by a Teflon or plastic ring. The sample (i.e., mRNA, peptides, or photoreleasable bioactive compounds) is first loaded into the microliter injector, which is then inserted into the microporator foot. The linear bearings are used to lower the foot onto the adherent cells. The sample is then injected into the center of the electroporation area shortly before the field pulse is applied. The injection must be slow to prevent shear damage to cells. Several seconds after pulse application, the foot is lifted off the cells, and the cells are washed three times with extracellular buffer.

Typically, electroporation was performed with rectangular pulses of field strengths from 200 to 340 V/cm applied for a 30–100-ms period. Using multiple pulses every 20–40 s and alternating the field direction between pulses were found to be effective in increasing the percentage of extracellular sample that is loaded (see also Tekle et al., 1991). Although efficient loading was achieved with rectangular pulses (Fig. 2), this device could also be used to generate exponential or oscillating pulse shapes from self-built or commercially available field stimulators. Fig. 1 *C* shows a schematic diagram of the circuit used to generate rectangular pulses. A large capacitor (10,000 μF) and a relay switch were used to generate nearly rectangular field pulses of up to several 100 ms duration (the resistance across the platinum electrodes in the microporator foot was ~330 Ω). An IBM-PC clone (486, 33 MHz) was used to control the three relays (on a Keithley-Metrabyte REL-16 relay board from Keithley Instruments, Cleveland, OH). The three relays have mercury amalgam contacts and are rated to 10 W at 0.5 A or 200 VDC max. The current across the electrodes was recorded via an A/D channel on a Keithley-Metrabyte DAS 8/PGA board. The monitored current can be used to verify the pulse form and to test whether the microporator foot is correctly positioned. (For more information on this microporator device, contact Dr. M. Teruel, teruel@acpub.duke.edu.)

Confocal imaging of calcium and membrane indicators

Because the microporator foot did not readily fit onto our microscope stage, closely spaced wire electrodes were used instead to apply field pulses to the adherent cells in experiments that involved rapid confocal imaging. These electrodes consisted of two platinum wires, 5 mm long and 3 mm apart, that were positioned parallel to the surface of the coverslip. The electrodes were then lowered to a minimal distance above the coverslip with a micromanipulator. The same electronics (Fig. 1 *C*) used to apply pulses to the microporator foot were used to apply pulses to these field electrodes. The 10,000 μF capacitor was large enough to produce nearly rectangular field pulses for this application.

The imaging system used to monitor the fluorescent indicators consisted of an inverted Nikon Diaphot microscope and a video-rate Odyssey confocal imaging system (Noran, Middleton, WI). The calcium indicator fluo-3 AM was excited at 488 nm, and the voltage-sensitive indicator di-8-ANEPPS was excited at 514 nm. A 150-MHz Pentium computer with 64 MB RAM, a Raptor imaging board (Bitflow, Woburn, MA), and Eye Image Calculator software (IO Industries, London, ON, Canada) was used to capture images every 16.7 ms from the previously mentioned confocal imaging system. A 3-ms timing pulse signaled the start of field application. To create the timing pulse, a computer-controlled shutter was opened to pass light from a UV laser (365 nm, Enterprise: Coherent, Palo Alto, CA). This generated a measurable signal in the confocal imaging system (the laser was coupled to the fluorescent port of the microscope). The captured images were analyzed with Image-1 software (Universal Imaging Corporation, Westchester, PA) and Eye Image Calculator software. The images were processed in several steps: background subtraction, low-pass filter

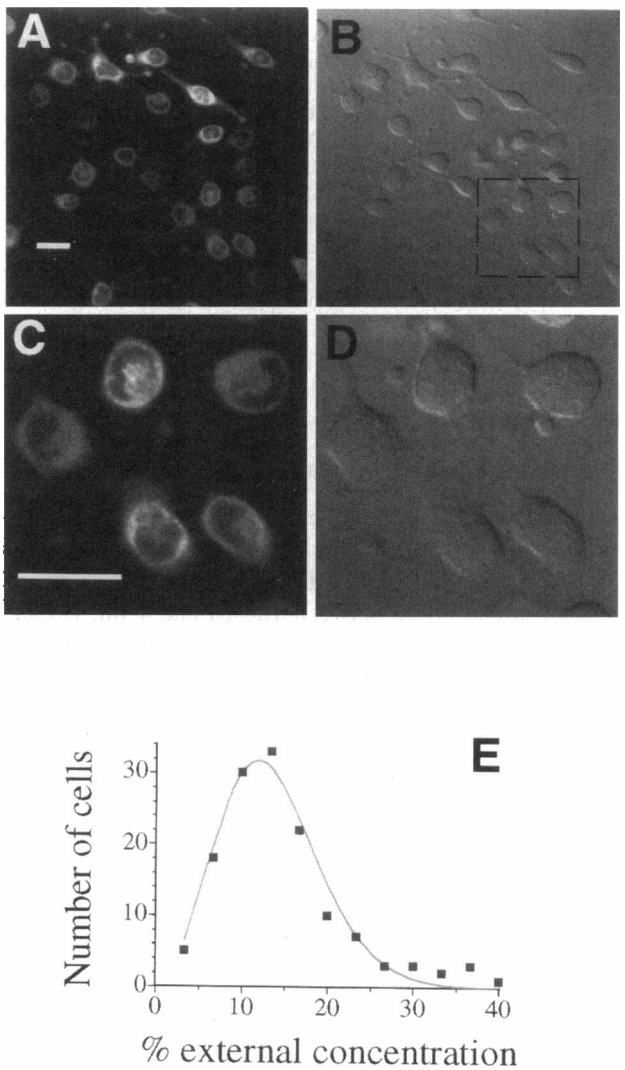

FIGURE 2 Loading of RBL cells with 500 kDa Calcium Green dextran, using two rectangular field pulses of 340 V/cm amplitude, of 30 ms duration, 40 s apart, and of opposite polarity. The calibration bar represents 20 μm. (*A*) Field of electroporated cells loaded with nuclear-excluded fluorescent dextran and imaged by confocal microscopy. (*B*) The same field of cells shown with confocal differential interference contrast (DIC) optics. (*C* and *D*) Confocal fluorescent and DIC images of a selected region of the images in *A* and *B*. The magnified region is indicated in *B* by dashed lines. (*E*) Histogram of the percentage of the external Calcium Green dextran concentration that was taken up by each cell. The approximate percentage of external Calcium Green concentration in the cytosol was determined by comparing the confocal fluorescent intensity of Calcium Green dextran in each cell with that of dilutions of the external Calcium Green dextran placed between two coverslips. The resulting loading profile is fit with a Poisson distribution.

(eight pixels, corresponding to ~0.9 μm), masking (rejection of intensities below a critical threshold), and ratioing to an averaged image (5–10 frames) collected before the start of poration to correct for uneven indicator distribution. In the measurements with fluo-3 AM, a line was drawn along the cell boundary in each ratioed image to more clearly show the shape of the cell. Before the di-8-ANEPPS images were processed, the background was subtracted.

The approximate percentage of external Calcium Green dextran concentration in the cytosol was determined by comparing the confocal fluo-

rescent intensity of Calcium Green dextran in each cell with that of dilutions of the external Calcium Green dextran placed between two coverslips. The relative concentration was corrected by a factor of 2 because the dilution series was made at saturating calcium concentrations, whereas the fluorescence intensity of Calcium Green dextran in the cells at basal calcium concentrations was 50% of maximum (as determined by ionomycin addition). The Calcium Green dextran (500,000 MW; catalog no. C-6766) was purchased from Molecular Probes.

Calibration of the membrane potential indicator di-8-ANEPPS was made by measuring the maximum gradient in fluorescent intensity during applied field pulses, and this was estimated to be a 10% relative fluorescence intensity change per 0.1 V (similar to the 9% per 0.1 V reported by Gross et al., 1986).

RESULTS

Small-volume electroporation of adherent cells

Electroporation devices typically require relatively large sample volumes because cells are usually electroporated in a cuvette or a cell chamber. Typical sample volumes used for electroporation are between 100 μl and 1 ml. Because only a few percent of the molecules of interest enter the cytosol during electroporation, the amount of sample needed for electroporation can be prohibitively expensive. To minimize the cost of in vitro transcribed RNA, recombinant protein, and other samples, we have developed an efficient electroporation device that uses only 1 μl of sample to load adherent cells in a 10-mm^2 surface area. A schematic representation of this small-volume electroporation device (microporator) is shown in Fig. 1 *A–D*. This device has been used for studying calcium responses from photorelease of caged inositol 1,4,5-trisphosphate (Oancea and Meyer, 1996), for studying the spatial dynamics of K-Ras by using mRNA transfection of green fluorescent protein (GFP) fusion constructs (Yokoe and Meyer, 1996), and for quantitative signal transduction studies with inhibitory peptides, protein domains, and GFP fusion proteins in different cell types.

Fig. 2 *A–D* show confocal fluorescent and differential interference contrast (DIC) images of adherent rat basophilic leukemia (RBL) cells that have been loaded with 500 kDa Calcium Green dextran with the microporator device. The field pulse protocol consisted of two rectangular pulses, 30 ms in duration, 340 V/cm in amplitude, 40 s apart, and of opposite polarity. Although this rectangular pulse protocol was efficient in electroporating the tested cell types, similar or higher loading levels might be achieved for particular cell types by using multiple pulse protocols or different ionic strengths, optimizing duration and field strength (Hui, 1995), or using other pulse shapes such as high frequency field stimulation (Chang, 1989). The 500-kDa size of the Calcium Green dextran that was loaded corresponds to the size of mRNA used in previous experiments (Yokoe and Meyer, 1996). As a test for viability, more than 90% of the loaded cells were found to exclude trypan blue 30 min after electroporation (N = 200). The loading of individual cells with dextran, expressed as a percentage of external concentration, is shown in a histogram in Fig. 2 *E*. The percentage of external concentration was determined by comparing the relative fluorescence inside the cells to that of a dilution series of the same sample between two coverslips. This procedure can be used for an approximate calibration because confocal microscopy can measure a fluorescence intensity that is nearly proportional to the local concentration of fluorophore. This is at least the case if the sample is thicker than the z axis resolution, which was ~2 μm in our measurements. For Fig. 2 *E*, we measured the fluorescence intensity from the brightest region of the cytosol, where the cell body is ~6–10 μm thick. Whereas most RBL cells were loaded by this protocol, the percentage loading with 500 kDa dextran varied between ~2–40% with an average loading of 12%. Surprisingly, we found that the percentage of external 500 kDa dextran that is loaded into the cells follows a nearly Poisson distribution, with more than 50% of the cells loading the dextran in a narrow range between 8% and 16% of the extracellular concentration. The shape of this distribution is consistent with the relative distribution of expressed GFP by RNA transfection described earlier (Yokoe and Meyer, 1996).

Field pulses induce individual calcium entry sites in the hyperpolarized region (plus pole) of adherent RBL cells and neuroblastoma cells

Electroporation-induced calcium entry into adherent cells was examined by using the fluorescent calcium indicator fluo-3 AM and rapid confocal microscopy. In all images in this study, the positive electrode (plus pole) is positioned to the left and the negative electrode (minus pole) to the right. Pulses of 167–340 V/cm in amplitude and 5–200 ms in duration were applied in the studies shown. Fig. 3 *A* shows a confocal image of an RBL cell before the field pulse was applied. To better visualize the influx of calcium, ratio images of the fluorescence intensity were used in Fig. 3 *B–G*. In the ratioed images, the fluorescence at each point is divided by the fluorescence at the same location before the field pulse was applied (average of 5–10 images). The contours of the cells are indicated by white lines. Fig. 3 *B–G* are ratio images taken ~33 ms after the start of a field pulse.

Strikingly, electric field pulses did not induce a uniform calcium entry across the plasma membrane, but instead induced a small number of local calcium entry sites. Fig. 3 *B–D* show examples of the observed local calcium entry sites recorded in neocortical neuroblastoma cells, and Fig. 3 *E–G* show examples of local calcium entry sites recorded in RBL cells. Most cells had only a limited number (one to a few) entry sites in the hyperpolarized regions (nearest the plus pole, where the membrane potential is negative during the applied field pulse). The formation of initial entry sites was often not restricted to the outermost tip of the processes, but also occurred at a limited number of locations along the processes, as well as at the hyperpolarized end of the cell body itself.

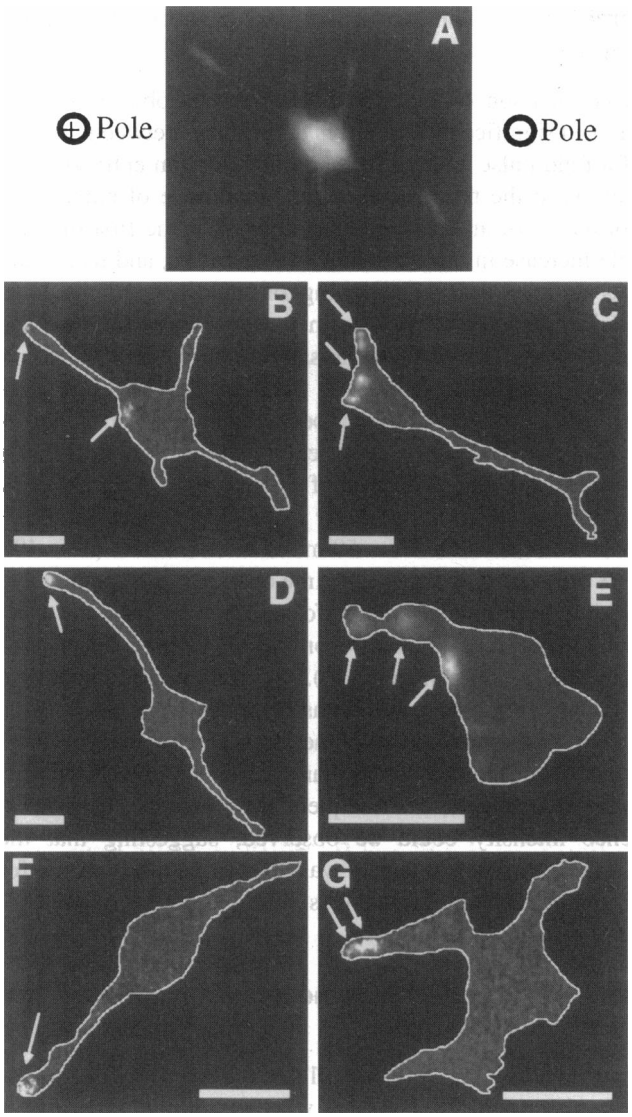

FIGURE 3 Formation of individual calcium entry sites in the hyperpolarized regions of cell body and processes. (*A*) Confocal fluorescence image of an RBL cell loaded with fluo-3 AM. (*B–D*) Masked and ratioed images of neocortical neuroblastoma cells taken 33 ms after the start of applied rectangular field pulses: 233 V/cm, 40 ms; 200 V/cm, 100 ms; and 167 V/cm, 200 ms, respectively. The light areas (*arrows*) indicate regions where significant calcium is entering the cell because of transiently formed entry sites created by the poration pulse. (*E–G*) Masked and ratioed images of RBL cells taken 33 ms after the start of applied rectangular field pulses: 267 V/cm, 124 ms; 400 V/cm, 100 ms; and 167 V/cm, 5 ms, respectively. Calibration bar is 20 μm.

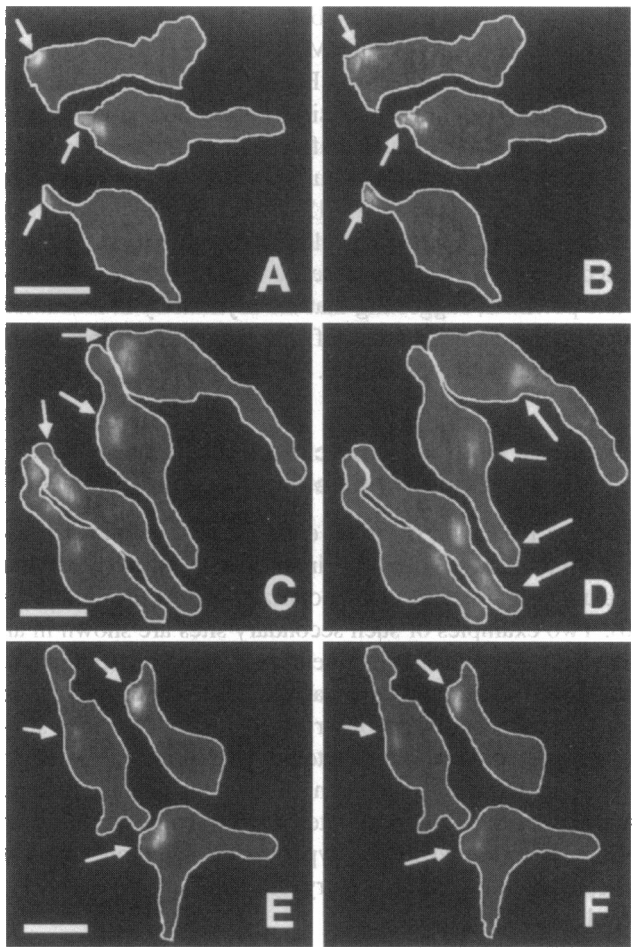

FIGURE 4 Asymmetry and reproducibility of calcium entry-site formation. (*A*) Entry-site formation in response to a first field pulse (267 V/cm, 40 ms). (*B*) The same field pulse was repeated 5 min later. Individual entry sites were formed at the same locations, suggesting that entry-site formation is not a stochastic process, but occurs at locations with a local membrane or cytoskeletal structure favorable for membrane disruption. (*C*) Entry-site formation in response to a first field pulse (267 V/cm, 40 ms). (*D*) The polarity of the field was switched before the application of a second field pulse with a shape identical to that of the field pulse applied in *C*. The location of the entry sites switched from left to right. (*E*) Entry-site formation in response to a first field pulse (267 V/cm, 40 ms). Cells are in standard extracellular buffer. (*F*) Entry-site formation after the exchange of the extracellular buffer with an intracellular one. The polar location of calcium entry sites was not affected by the presence or absence of a basal plasma membrane potential, suggesting that the asymmetry in entry-site formation is not the result of a superposition of basal and applied membrane potentials. The calibration bar represents 20 μm.

Sequential field pulses lead to the formation of calcium entry sites at identical sites, independently of the basal membrane potential

Surprisingly, when the same field pulse was repeated after a cell had recovered from a first pulse (>5 min), individual calcium entry sites were formed at the same locations (Fig. 4, *A* and *B*). This finding, observed in 12 out of 12 cells, suggests that the formation of entry sites is not a stochastic process, but occurs at locations with a local membrane or cytoskeletal structure favorable for membrane disruption. Calcium entry sites were formed in the opposite cell region when the polarity of the field was switched (Fig. 4, *C* and 4 *D*; $N = 12$ out of 12).

It has been proposed that the superposition of the basal membrane potential and the applied membrane potential may contribute to an asymmetrical permeabilization of cells (Mehrle et al., 1985; Tekle et al., 1990). We tested this hypothesis by applying a field pulse while the basal membrane potential was eliminated. This was achieved by replacing the normal extracellular buffer on the outside of the

cells with an "intracellular" buffer (135 mM KCl, 5 mM NaCl, 1.5 mM $CaCl_2$, 20 mM HEPES (pH 7.4), 1.5 mM $MgCl_2$, and 10 mM glucose). Fig. 4, *E* and *F*, compares the formation of calcium entry sites before and after the exchange of the extracellular buffer with an intracellular one. In control experiments, the buffer was switched before the first pulse was applied. In 12 out of 12 cells (for each condition), the location of calcium entry sites was not affected by the presence or absence of a basal plasma membrane potential, suggesting that the asymmetry in formation of entry sites is not a result of a superposition of basal and induced membrane potentials.

Formation of smaller calcium entry sites at the depolarized end of the cell (minus pole)

After the formation of initial entry sites in the hyperpolarized region, most cells also induced one or more smaller calcium entry sites at the depolarized end of the cell (N = 40). Two examples of such secondary sites are shown in an RBL cell (Fig. 5 *A*) and a neuroblastoma cell (Fig. 5 *B*). Interestingly, the entry sites at the depolarized end of the cell were almost always observed only after the entry sites at the hyperpolarized end started to grow. Not only was the magnitude of the local calcium influx at the depolarized end smaller, but the number of sites was typically smaller than the number formed in the hyperpolarized region. In most cells, only one calcium entry site was observed at the depolarized end.

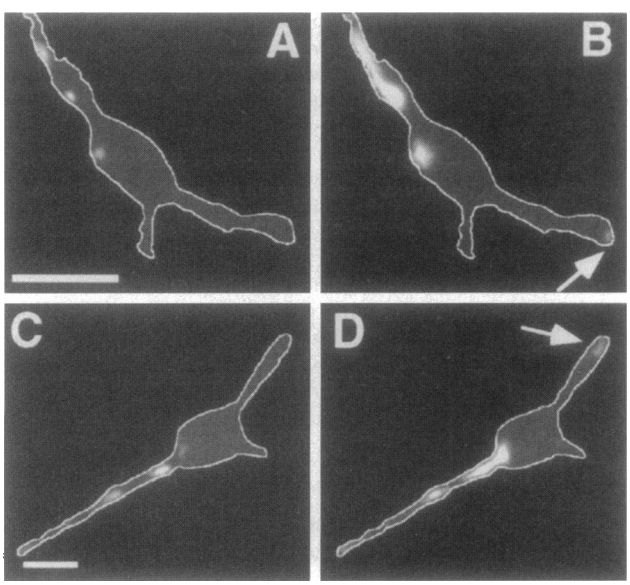

FIGURE 5 Formation of secondary calcium entry sites at the depolarized ends of cells. (*A* and *B*) Masked and ratioed images of an RBL cell at 33 and 67 ms, respectively, after the start of a field pulse (267 V/cm, 34 ms). Secondary entry-site formation is indicated in *B* by an arrow. (*C* and *D*) Masked and ratioed images of a neocortical neuroblastoma cell at 33 and 67 ms, respectively, after the start of a field pulse (233 V/cm, 40 ms). Secondary entry-site formation is indicated in *D* by an arrow. The calibration bar represents 20 μm.

Time course for formation and closure of calcium entry sites

A comparison of individual RBL or neuroblastoma cells showed significant differences in the delay between the start of a field pulse and the formation of calcium entry sites, as well as in the time required for the closure of entry sites. Formation of an entry site was defined as the first measurable increase in local calcium concentration, and its closure was defined as the beginning of a decline in the local calcium concentration. The increase in local fluorescence intensity was not sufficient to saturate the calcium indicator, which enabled us to monitor the formation of entry sites throughout the measurement period. Fig. 6, *A* and *B*, shows examples of calcium entry sites that closed in less than 1 s (see arrows). The formation of calcium entry sites typically occurred after an initial delay of 17–33 ms, and entry site closure times varied from 50 ms to more than 1 s (N = 40).

A different analysis of the time course of the opening and closing of entry sites was performed by recording the average fluorescence intensity from a cell before, during, and after electroporation (N = 20). Fig. 6 *C* shows an example of relative fluorescence intensity traces from three cells. Although the sharp rise in the fluorescence intensity was typically terminated in less than 1 s, in many instances (i.e., lower two traces), a subsequent slow increase in fluorescence intensity could be observed, suggesting that the plasma membrane integrity was not completely restored for a time period longer than 10 s.

Recovery of calcium homeostasis after electroporation

Knowing how long it takes cells to recover from electroporation is critical for assessing whether cellular experiments can readily be performed after electroporation. We investigated the integrity of the plasma membrane after the formation of calcium entry sites by measuring the recovery of the average calcium concentration to its basal level from before electroporation. Fig. 7 shows examples of such recovery traces. In most cells, within 1–2 min, baseline calcium concentration was lowered to a concentration that was within 20% of the prepulse baseline calcium concentration. After 10 min, the recovery was usually within 10% of the prepulse calcium concentration (for a basal calcium concentration of ~100 nM, the level would be restored to 100 nM < $[Ca^{2+}]$ < 110 nM). We had found earlier that FcεRI (antigen receptor)-induced calcium spikes in RBL cells can be triggered equally well before electroporation and 1 min after electroporation, demonstrating that receptor-mediated Ca^{2+} signaling is not significantly perturbed by electroporation (T. Stauffer and T. Meyer, unpublished observations). These receptor-induced calcium responses require that several membrane-localized signaling molecules be intact immediately after electroporation (the two tyrosine kinases Lyn and Syk, as well as phospholipase C γ, are required for the response; Jouvin et al., 1995).

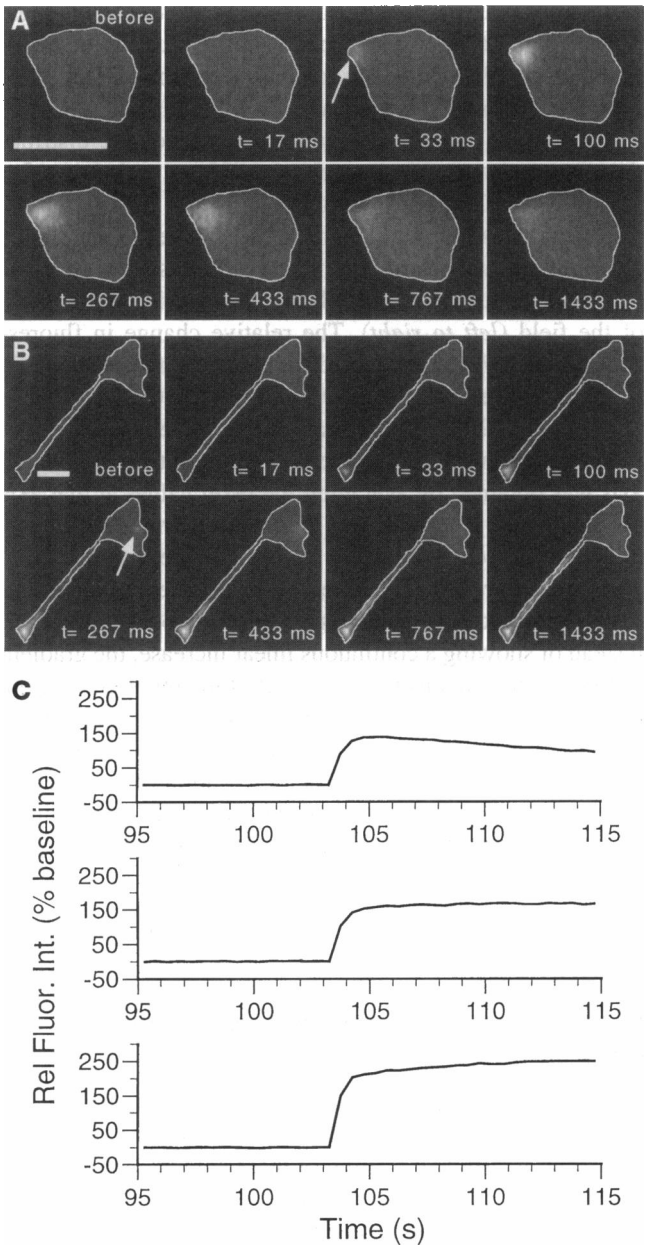

FIGURE 6 Time course for the formation and closure of calcium entry sites. (*A*) Example of a local calcium entry event that was terminated rapidly (*arrow*). A field pulse of 200 V/cm amplitude and 17 ms duration was used. (*B*) Example of a local calcium entry event that remained open for ~1 s (*arrow*). A field pulse of 167 V/cm amplitude and 200 ms duration was used. Calcium entry could typically only be observed only after an initial delay of 17–33 ms. The closure time for calcium entry sites varied from between 50 ms to a few seconds after the pulse was terminated (N = 40). The calibration bar represents 20 μm. (*C*) Measurement of the change in the overall calcium permeabilization of a cell during application of individual field pulses. The average change in the fluorescence intensity of individual RBL-cells is shown before, during, and after the application of a 333 V/cm, 40-ms pulse.

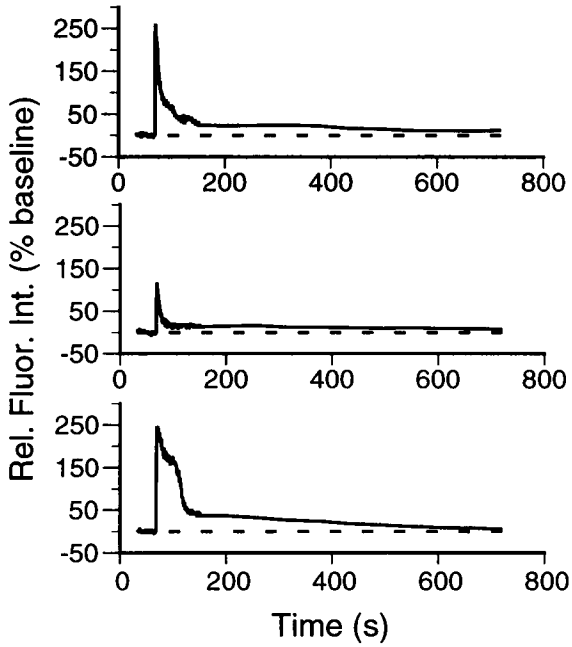

FIGURE 7 Recovery of basal cytosolic free calcium concentration after electroporation. Calcium entry sites typically close within a few seconds. The cytosolic calcium concentration is recovered to 10% of baseline within 10 min of electroporation. The examples shown are RBL cells before, during, and after a 330 V/cm, 40-ms field pulse.

Local differences in membrane potential during electrical field application

The preferential formation of calcium entry sites at the plus pole of the cell compared to the minus pole could result from different absolute values of the membrane potential at the two poles due to different relative ion permeabilities. Alternatively, the absolute values of the membrane potentials could be the same at the two poles, but a negative membrane potential, as opposed to a positive one, could cause larger entry sites to form. If the plasma membrane were to behave as an ideal membrane with a small nonselective membrane ion permeability, one would expect that the applied electric field generates a symmetrical, linearly increasing membrane potential from the plus pole to the minus pole. At the outermost left end of the cell (plus pole), the membrane potential should be maximally negative or hyperpolarized. At the outermost right end of the cell (minus pole), the membrane potential should be maximally positive or depolarized. For a field strength of 200 V/cm, a symmetrical cell that extends its processes over 60 μm in the direction of the field should experience membrane potentials from -0.6 V at the left to $+0.6$ V at the right.

The membrane potential during such a pulse protocol was measured by using the voltage indicator di-8-ANEPPS. Fluorescent images were taken every 17 ms before, during, and after the field pulse was applied. Fig. 8 *A* shows an example of such an experiment using a false color scale. Images taken before pulse application, as well as 17 ms and 33 ms after the start of the 100-ms field pulse, are shown. Individual images were masked and divided by an averaged image taken before the field pulse to calibrate the relative changes in membrane potential. Indeed, in all images, the membrane potential between the plus and minus poles grad-

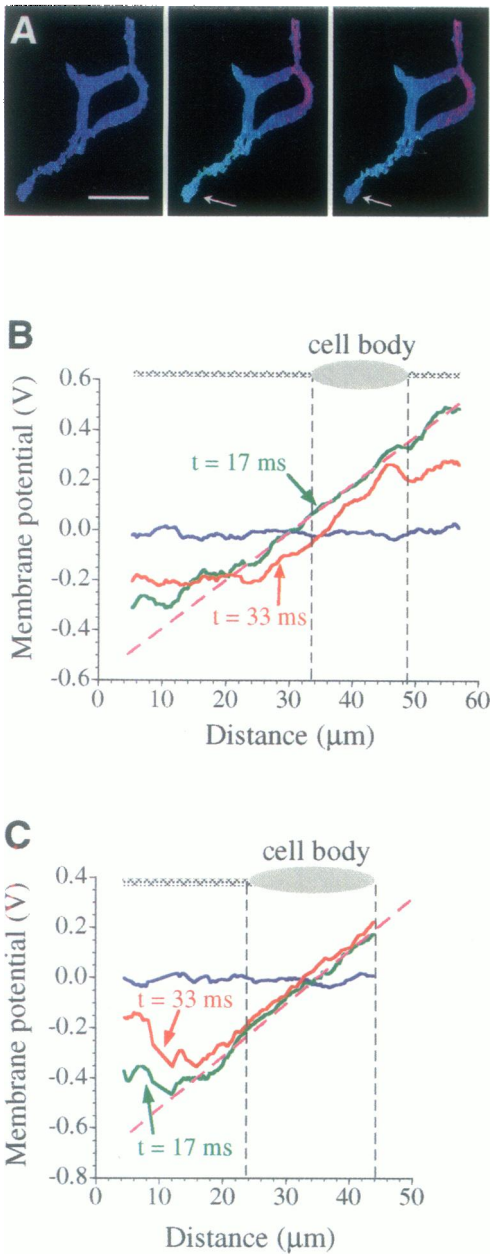

FIGURE 8 Membrane potential changes during field pulses measured with the voltage indicator di-8-ANEPPS. (*A*) Change in membrane potential in an RBL cell subjected to a 200-V/cm, 100-ms field pulse. The membrane potential increases from the plus to minus pole (*left to right in each panel*). The left panel shows the membrane potential before application of the field pulse. The two right panels show the membrane potential 17 ms and 33 ms after the start of the field pulse. An apparent reduction in the local membrane potential can be observed between the images (*arrow*). No significant changes in the voltage distributions were observed in images taken 33 ms or longer after the start of a field pulse. The calibration bar is 20 μm. (*B* and *C*) Quantitative analysis of the relative plasma membrane fluorescence change as a function of location in the direction of the field (*left to right*; plus pole to minus pole). Each point along the cell axis was obtained by averaging the pixel values at that axis position and by normalizing the resulting value to the average fluorescence intensity before the field application. Maximum slopes were typically observed in the cell body. The membrane potential leveled of at the outer ends of filopodia at membrane voltages that corresponded to a variable transmembrane voltage of ±0.2–0.5 V.

ually increased from a negative to a positive membrane potential. In some experiments a local reduction in membrane potential could be observed between the images taken 17 ms and 33 ms after the start of a field pulse (e.g., Fig. 8 *A*, *arrow*). No significant changes in the voltage distributions were observed in images taken 33 ms or longer after the start of a field pulse (data not shown).

To more quantitatively monitor the changes in membrane potential, an analysis of the relative fluorescence increase was made as a function of relative location in the direction of the field (*left to right*). The relative change in fluorescence intensity was converted to an approximate change in transmembrane voltage (~10% change per 0.1 V; see also Gross et al., 1986). Fig. 8, *B* and *C*, shows examples of the voltage distribution in two cells. Each point along the cell axis was obtained by averaging the pixel values at that axis position and by normalizing the resulting value to the average fluorescence intensity before the field application. The voltage gradients obtained by this procedure were typically observed to be steepest in the cell body. However, instead of showing a continuous linear increase, the gradient in fluorescence intensity leveled off at the outer ends of the cell to values that corresponded to a transmembrane voltage of ±0.2–0.5 V. The value at which the plateau was reached was variable between cells. The observation of a plateau of the membrane potential at both poles is consistent with a partial breakdown of the transmembrane potential at values higher than ±0.2–0.5 V.

DISCUSSION

Formation of a limited number of calcium entry sites

We investigated electric field-induced calcium entry in adherent mammalian cells by using the same pulse protocols that result in efficient loading of these cells with macromolecules while retaining more than 90% cell survivability. These pulse protocols, consisting of rectangular pulses of 167–340-V/cm amplitude and 5–200-ms duration, lead to the formation of a few individual calcium entry sites, preferentially in the hyperpolarized membranes of the cell body and processes. In adherent cells without processes, similar entry sites were also observed (e.g., Fig. 6 *A*). The relative loading of dextran by individual cells could best be described by a Poisson distribution (Fig. 2), an observation that is consistent with the hypothesis that not only calcium ions, but also macromolecules, enter the cell only through a limited number of sites. The discrete nature of these local calcium entry sites suggests that they reflect the opening of individual large pores. Studies by Chang and Reese (1990), using rapid-freezing electron microscopy, observed large pores of 20–120 nm after electroporation, but at a significantly higher density than the density of calcium entry sites observed in our study. Discrete local calcium entry sites were not observed in an earlier nonconfocal light microscopy study of electric field-induced calcium influx into

oocytes (Kinosita et al., 1991). This may be explained by the lower spatial resolution of their study compared to the present study, or may suggest that, as in the study of Chang and Reese (1990), a much higher density of calcium entry sites was present. A higher density of macromolecule entry sites may be the result of using a higher field strength, different cell types, or buffers with different salt concentrations.

We found that the plasma membrane potential in both polar regions of adherent cells partially collapsed immediately after electric field application. These results are consistent with earlier studies of the collapse of the membrane potential in sea urchin eggs (Hibino et al., 1993). In that study, a submicrosecond collapse of the membrane potential to about ±0.7 V was observed in the two polar regions of the egg. During the next 1000 μs, the membrane potential continued to collapse to about −0.3 V in the region at the plus pole and to about +0.5 V at the minus pole. This rapid breakdown in membrane potential is likely a result of the formation of small pores on the time scale of microseconds (Freeman et al., 1994).

In our studies, the formation of individual calcium entry sites occurs after the partial collapse of the plasma membrane potential at the two poles. Entry sites were often distributed over a significant region of the cell body and processes facing the plus pole, which could be explained by the observed plateau in the membrane potential over similar large regions (Fig. 8, *B* and *C*). The forces required for the formation of entry sites may be equally strong throughout these plateau regions. This suggests that a two-step process is responsible for the formation of localized calcium entry sites (Fig. 9 *A*; see also other two-step models for pore formation by Kinosita and Tsong, 1977b; Tsong, 1991; Chang and Reese, 1990; Zhelev and Needham, 1994). In a model consistent with our results, the application of an electric field leads to a rapid increase in the transmembrane potentials at the two poles of a cell. As the absolute value of the membrane potential at the two poles increases above a threshold of about +0.7 to 1 V and −0.7 to 1 V, small pores are formed on a microsecond time scale (Hibino et al., 1993). These small pores then reduce the membrane potential to approximately ±0.2–0.5 V in both polar regions of the cell. Thus the membrane potential in both polar regions reaches a plateau that remains present throughout the application of the electric field pulse (17–340 ms in our studies). The absolute value of the membrane potential (~0.2–0.5 V) is significantly higher than the basal membrane potential (~−0.08 V). The resulting continued force exerted on electric charges present in the plasma membrane would then lead to the second step: the formation of large calcium entry sites over a time period of tens of milliseconds. These calcium entry sites are likely defined by the cytoskeleton or by the local membrane structure, because the repeated application of the same field pulse leads to calcium entry at the same locations. For example, studies by Rols and Teissie (1992) have found evidence for cytoskeletal involvement in mammalian cell electroporation.

Time course for closure of calcium entry sites

We found that calcium entry sites, formed at both the depolarized and hyperpolarized ends of cells, remained open for variable time periods that ranged from ~50 ms to a few seconds. Baseline calcium concentration was recovered to less than 20% of the preelectroporation levels within 1 or 2 min and within 10% of the preelectroporation levels within 10 min. Thus the resealing process in our studies has at least two time constants. The calcium entry sites closed on the time scale of seconds, and there was some residual membrane leakiness due to small pores that remain open on the time scale of minutes. The time we observed for calcium entry site closure is fast compared to other studies in which the closure of electropores to macromolecules took minutes to hours, even at temperatures greater than 21°C (e.g., Serpersu et al., 1985; Kinosita and Tsong, 1977a; Kinosita et al., 1992; Rols and Teissie, 1992). The fast closure time observed in our electroporation protocol probably does not depend on the type of adherent cell used, because we found the same time scale in two different types of cells. However, the faster closure time in our studies may result partially from the fact that many other studies used cells in suspension that have a cytoskeletal organization that is very different from that of adherent cells. Pore resealing times have been found to be dependent on cytoskeletal structure (Rols and Teissie, 1992). Moreover, in our studies we used low-amplitude, long-duration field pulses, as well as other conditions suitable for the electroporation of adherent mammalian cells. In many of the other studies, microsecond-long pulses of very high field strength were used, as well as different buffer compositions. These differences in electroporation conditions may contribute to different rates of pore closure.

In another test of membrane resealing, we have shown that 90% of the observed cells were sealed 30 min after electroporation, as determined by trypan blue exclusion. Furthermore, they were also morphologically intact, as judged by inspection by differential interference microscopy. In addition, even though there is some residual membrane leakiness through small pores that remain open for many minutes after the calcium entry sites close, receptor-mediated signal transduction was intact within 1 min of electroporation.

Asymmetry of electroporation

In our study, the individual calcium entry sites were located preferentially in the cell region facing the positive electrode where the membrane potential is hyperpolarized (more negative). When the polarity of the applied field was reversed, the location of the entry sites also reversed to always be on the hyperpolarized part of the cell. It has been proposed that the asymmetry in entry site formation is due to higher amplitude membrane potentials at the plus pole than at the minus pole, resulting from a superposition of the basal and induced membrane potentials (Mehrle et al., 1985; Tekle et

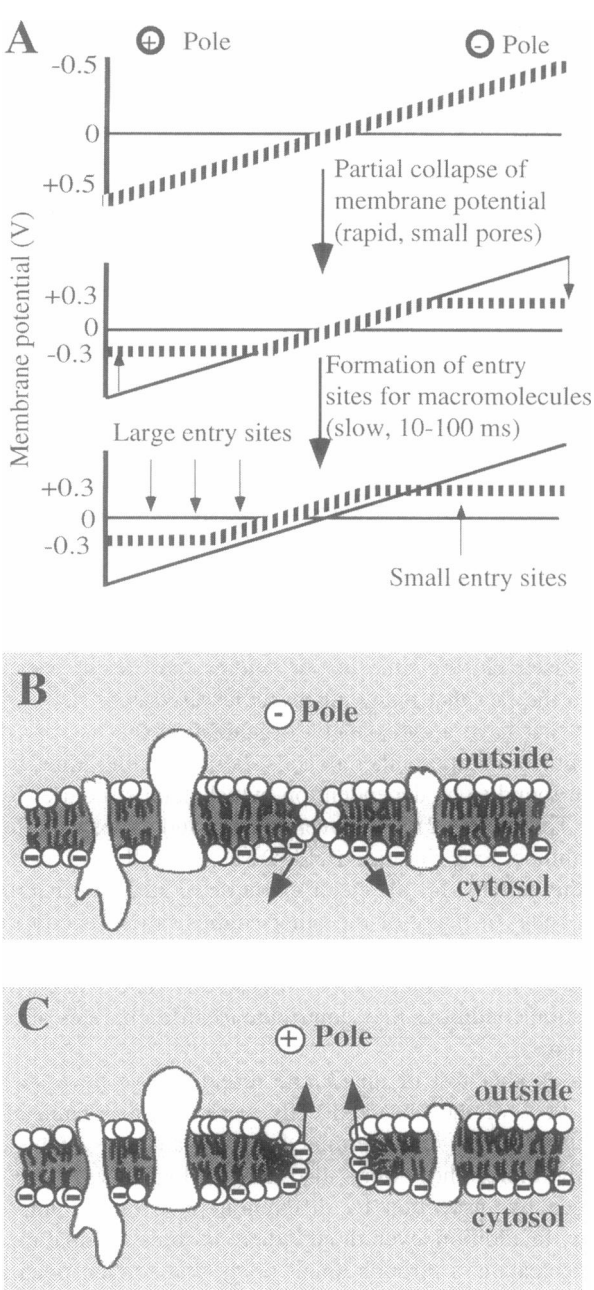

FIGURE 9 (*A*) Idealized two-step model for the formation of entry sites for macromolecules that explains the results in Fig. 8. In an initial rapid step (μs to ms), small pores are formed at both the hyperpolarized and depolarized ends of cells, which reduce the peak membrane potentials to values of approximately $\pm$0.2–0.5 V. These small pores do not lead to a measurable calcium influx. After a delay of typically more than 17 ms, a few pores grow sufficiently large to allow for the entry of macromolecules. The resulting entry sites are predominantly in the hyperpolarized ends of cells and are defined by the local membrane structure. One to a few smaller entry sites are also formed at the depolarized end of the cell. Depending on the number of pores and entry sites open at a given time in different regions of the cell, the shape of the membrane potential gradient can shift during the application of the field pulse (see Fig. 8, *B* and *C*). (*B* and *C*) Model explaining the polar asymmetry in the formation of entry sites for macromolecules. Charge asymmetry between the inner and outer leaflets of the membrane is likely responsible for the asymmetry in the formation of entry sites at the plus and minus poles. Most negatively charged lipids are found in the inner leaflet of the plasma membrane. In *B*, small entry sites are formed at the depolarized ends of cells because the electric field prevents negatively charged lipid headgroups from entering the bilayer. In *C*, large entry sites are formed at the hyperpolarized end of the cell because the applied field exerts a strong force on the negatively charged lipid headgroups, favoring their insertion into and across the bilayer. Once the bilayer is disrupted, the repulsive force between the inserted negatively charged lipid headgroups may help to enlarge and stabilize aqueous pores in the plasma membrane.

al., 1990; Djuzenova et al., 1996). However, we did not find this to be the case. Entry site formation still occurred preferentially at the hyperpolarized end, even when the basal plasma membrane potential was eliminated by replacing the extracellular medium with an intracellular one.

The asymmetry in the formation of calcium entry sites could be a result of the positive charge of the calcium ions. Earlier studies suggested that the movement of molecules through electropores can be driven by electroosmosis (Dimitrov and Sowers, 1990; Sowers, 1988) or electrophoresis (Sukharev et al., 1992). During the experimental conditions used in our studies, the rate of calcium influx was not significantly different during and immediately after the application of a rectangular electric pulse of 17–300 ms. Because the driving force of the electric field is only present during application of the field pulse, our experimental observations are more consistent with a calcium influx that results mostly from passive diffusion and not from active processes like electroosmosis and electrophoresis.

Overall, our observation that preferential electropermeabilization occurs at the plus pole of the cell is consistent with the finding of other groups (Merhle et al., 1985; Rossignol et al., 1983; Tekle et al., 1990, 1991). However, different studies reported a higher permeabilization at the minus pole compared to the plus pole (Sowers et al., 1988; Hibino et al., 1991, 1993). In two studies, the site of high permeabilization was found to switch according to the salt concentration and osmotic pressure of the buffer used (Tekle et al., 1994; Djuzenova et al., 1996). Furthermore, different pole preferences for permeabilization were observed as a function of the size of the electroporated macromolecules (Tekle et al., 1994). Together, these findings suggest that the polar nature of the electroporation process is dependent on the buffer composition and the pulse protocol, as well as other parameters, such as the cell type and size of macromolecule used. Further studies are needed to understand the properties of the plasma membrane that can explain these different results.

Our model, as shown in Fig. 9 *A* and earlier in the Discussion, predicts the formation of macromolecule entry sites at both poles, but it does not explain how asymmetry in entry site formation can be generated between the plus and minus poles. A possible major reason for the asymmetry may be that the inner, cytosolic leaflet of the plasma membrane has a higher concentration of negatively charged lipids than the outer leaflet of the plasma membrane (i.e., Whatmore and Allan, 1994). As shown in the schematic

model in Fig. 9, *B* and *C*, the asymmetrical force that is likely exerted on the negative charged lipids at the two poles of the cell could account for the greater effectiveness of hyperpolarization compared to depolarization in inducing the observed calcium entry sites. In the depolarized part of the cell (Fig. 9 *B*), the applied field keeps the negatively charged lipid headgroups away from the lipid bilayer. However, in the hyperpolarized part of the cell (Fig. 9 *C*), the applied field exerts a strong force on the negatively charged lipid headgroups, favoring their insertion into the bilayer. Once the bilayer is disrupted, the repulsive force between the inserted negatively charged lipid headgroups may lead to growing aqueous pores in the plasma membrane. Although this model can explain the observed asymmetry in permeabilization in our studies, the different observation in the polarity of electropermeabilization described above suggests that several factors in addition to the lipid asymmetry contribute to the processes of formation of calcium entry sites and their rapid closure.

CONCLUSIONS

Our study showed that low-amplitude, long-duration rectangular field pulses, useful for the efficient loading of adherent cells, generate only a limited number of calcium entry sites, preferentially in the hyperpolarized region of the cell. Surprisingly, the formation of these entry sites was not a stochastic process. Instead, the sites of calcium entry were the same when the applied pulse protocol was repeated. This suggests that the local composition of the plasma membrane, cytoskeleton components, or local cell adhesion define a specific number of sites where hyperpolarizing membrane potentials can lead to preferential membrane disruption and transient formation of entry sites. Further studies will be needed to investigate the structural basis that defines the location of these sites. Together with earlier studies on electroporation, our experiments suggest that the entry of macromolecules into adherent cells is enabled by a two-step process that begins with the rapid formation of small pores. These small pores increase the permeability of the plasma membrane to small ions, leading to a partial breakdown of the membrane potential at both poles, which is followed by the slower opening of a limited number of transient large entry sites in the hyperpolarized part of cells. Plasma membrane resealing is also a two-step process, with macromolecule entry sites resealing on a time scale of 50 ms to several seconds and residual small pores remaining open for several minutes. The asymmetry in permeabilization may result from the asymmetry of negatively charged lipids that are preferentially localized in the cytosolic leaflet of the plasma membrane.

We thank Drs. B. Goldsmith and C. Martenson for designing excellent prototypes of the microporator; D. Poe for skillful machining of the device; and Dr. T. Stauffer, Dr. J. Horne, E. Oancea, H. Yokoe, Dr. K. Subramanian, and K. Shen for patient testing of the device and the electroporation protocols and for contributing valuable ideas on how to improve them. We are also grateful to Drs. D. Needham and D. Raucher for comments on the manuscript and Dr. J. Chun (UCSD) for providing the neuroblastoma cells.

This work was supported by National Institutes of Health grants GM-48113 and GM-51457. TM was supported by a fellowship from the David and Lucille Packard Foundation.

REFERENCES

Baum, C., P. Forster, S. Hegewisch-Becker, and K. Harbers. 1994. An optimized electroporation protocol applicable to a wide range of cell lines. *Biotechniques.* 17:1058–1062.

Boitano, S., E. R. Dirksen, and M. J. Sanderson. 1992. Intercellular propagation of calcium waves mediated by inositol trisphosphate. *Science.* 258:292–295.

Chang, D. C. 1989. Cell fusion and cell poration by pulsed radio-frequency electric fields. *Biophys. J.* 56:641–652.

Chang, D. C., B. M. Chassy, J. A. Saunders, and A. E. Sowers, editors. 1992. Guide to Electroporation and Electrofusion. Academic Press, San Diego, CA.

Chang, D. C., and T. S. Reese. 1990. Changes in membrane structure induced by electroporation as revealed by rapid-freezing electron microscopy. *Biophys. J.* 58:1–12.

Chun, J., and R. Jaenisch. 1996. Clonal cell lines produced by infection of neocortical neuroblasts using multiple oncogenes transduced by retroviruses. *Mol. Cell. Neurosci.* 7:304–321.

Dimitrov, D. S., and A. E. Sowers. 1990. Membrane electroporation—fast molecular exchange by electroosmosis. *Biochim. Biophys. Acta.* 1022: 381–392.

Djuzenova, C., U. Zimmermann, H. Frank, V. L. Sukhorukov, E. Richter, and G. Fuhr. 1996. Effect of medium conductivity and composition on the uptake of propidium iodide into electropermeabilized myeloma cells. *Biochim. Biophys. Acta.* 1284:143–152.

Freeman, S. A., M. A. Wang, and J. C. Weaver. 1994. Theory of electroporation of planar bilayer membranes: predictions of the aqueous area, change in capacitance, and pore-pore separation. *Biophys. J.* 67:42–56.

Gross, D., L. M. Loew, and W. W. Webb. 1986. Optical imaging of cell membrane potential changes induced by applied electric fields. *Biophys. J.* 50:339–348.

Hibino, M., H. Itoh, and K. Kinosita, Jr. 1993. Time courses of cell electroporation as revealed by submicrosecond imaging of transmembrane potential. *Biophys. J.* 64:1789–1800.

Hibino, M., M. Shigemori, H. Itoh, K. Nagayama, and K. Kinosita, Jr. 1991. Membrane conductance of an electroporated cell analyzed by submicrosecond imaging of transmembrane potential. *Biophys. J.* 59: 209–220.

Hui, S. W. 1995. Effects of pulse length and strength on electroporation efficiency. *In* Methods in Molecular Biology, Vol. 48: Animal Cell Electroporation and Electrofusion Protocols. J. A. Nickoloff, editor. Humana Press, Totowa, NJ. 93–113.

Jouvin, M. H., R. P. Numerof, and J. P. Kinet. 1995. Signal transduction through the conserved motifs of the high affinity IgE receptor FcεRI. *Semin. Immunol.* 7:29–35.

Kinosita, K., Jr., M. Hibino, H. Itoh, M. Shigemori, K. Hirano, Y. Kirino, and T. Hayakawa. 1992. Events of membrane electroporation visualized on a time scale from microsecond to seconds. *In* Guide to Electroporation and Electrofusion. D. C. Chang, B. M. Chassy, J. A. Saunders, and A. E. Sowers, editors. Academic Press, San Diego, CA. 29–46.

Kinosita, K., Jr., H. Itoh, S. Ishiwata, K. Hirano, T. Nishizaka, and T. Hayakawa. 1991. Dual-view microscopy with a single camera. Real-time imaging of molecular orientations and calcium. *J. Cell Biol.* 115: 67–73.

Kinosita, K., Jr., and T. Y. Tsong. 1977a. Formation and resealing of pores of controlled sizes in human erythrocyte membrane. *Nature.* 268: 438–441.

Kinosita, K., Jr., and T. Y. Tsong. 1977b. Voltage-induced pore formation and hemolysis of human erythrocytes. *Biochim. Biophys. Acta.* 471: 227–242.

Kinosita, K., Jr., and T. Y. Tsong. 1979. Voltage-induced conductance in human erythrocyte membranes. *Biochim. Biophys. Acta.* 554:479–497.

Maurel, P., L. Gualandris-Parisot, J. Teissie, and A. M. Duprat. 1989. Electric-field-induced permeabilization and fusion of embryonic amphibian cells. *Exp. Cell Res.* 184:207–218.

Mehrle, W., U. Zimmermann, and R. Hampp. 1985. Evidence for asymmetrical uptake of fluorescent dyes through electro-permeabilized membranes of *Avena* mesophyll protoplasts. *FEBS Lett.* 185:89–94.

Oancea, E., and T. Meyer. 1996. Reversible desensitization of inositol trisphosphate-induced calcium release provides a mechanism for repetitive calcium spikes. *J. Biol. Chem.* 271:17253–17260.

Raptis, L. H., K. L. Firth, H. L. Brownell, A. Todd, W. C. Simon, B. M. Bennett, L. W. MacKenzie, and M. Zannis-Hadjopoulos. 1995. Electroporation of adherent cells in situ for the introduction of nonpermeant molecules. *In* Methods in Molecular Biology, Vol. 48: Animal Cell Electroporation and Electrofusion Protocols. J. A. Nickoloff, editor. Humana Press, Totowa, NJ. 93–113.

Rols, M., and J. Teissie. 1992. Experimental evidence for the involvement of the cytoskeleton in mammalian cell electropermeabilization. *Biochim. Biophys. Acta.* 1111:45–50.

Rossignol, D. P., G. L. Decker, W. J. Lennarz, T. Y. Tsong, and J. Teissie. 1983. Induction of calcium-dependent, localized cortical granule breakdown in sea urchin eggs by voltage pulsation. *Biochim. Biophys. Acta.* 763:346–355.

Serpersu, E. J., K. Kinosita, Jr., and T. Y. Tsong. 1985. Reversible and irreversible modification of erythrocyte membrane permeability by electric field. *Biochim. Biophys. Acta.* 812:779–785.

Shigekawa, K., and W. J. Dower. 1988. Electroporation of eukaryotes and procaryotes: a general approach to the introduction of macromolecules into cells. *BioTechniques.* 6:742–751.

Sowers, A. E. 1984. Characterization of electric field-induced fusion of erythrocyte ghost membranes. *J. Cell Biol.* 99:1989–1996.

Sowers, A. E. 1988. Fusion events and nonfusion contents mixing events induced in erythrocyte ghosts by an electric pulse. *Biophys. J.* 54: 619–626.

Sowers, A. E. 1995. Permeability alteration by transmembrane electric fields: electroporation. *In* Permeability and Stabiliity of Lipid Bilayers. E. A. Disalvo and S. A. Simon, editors. CRC Press, Boca Raton, FL. 105–121.

Sukharev, S. I., V. A. Klenchin, S. M. Serov, L. V. Chernomordik, and Y. A. Chizmadzhev. 1992. Electroporation and electrophoretic DNA transfer into cells. *Biophys. J.* 63:1320–1327.

Teissie, J., V. P. Knutson, T. Y. Tsong, and M. D. Lane. 1982. Electric-pulse induced fusion of 3T3 cells in monolayer culture. *Science.* 216: 537–538.

Tekle, E., R. D. Astumian, and P. B. Chock. 1990. Electro-permeabilization of cell membranes: effect of the resting membrane potential. *Biochem. Biophys. Res. Commun.* 172:283–287.

Tekle, E., R. D. Astumian, and P. B. Chock. 1991. Electroporation by using bipolar oscillating electric field: an improved message for DNA transfection of NIH 3T3 cells. *Proc. Natl. Acad. Sci. USA.* 88:4230–4234.

Tekle, E., R. D. Astumian, and P. B. Chock. 1994. Selective and asymmetric molecular transport across electroporated cell membranes. *Proc. Natl. Acad. Sci. USA.* 91:11512–11516.

Tsong, T. Y. 1991. Electroporation of cell membranes. *Biophys. J.* 60: 297–306.

Whatmore, J. L., and D. Allan. 1994. Phospholipid asymmetry in plasma membrane vesicles derived from BHK cells. *Biochim. Biophys. Acta.* 1192:88–94.

Yang, T., W. C. Heiser, and J. Sedivy. 1995. Efficient in situ electroporation of mammalian cells grown on microporous membranes. *Nucleic Acids Res.* 23:2803–2810.

Yokoe, H., and T. Meyer. 1996. Spatial dynamics of GFP-tagged proteins investigated by local fluorescence enhancement. *Nature Biotechnol.* 14:1252–1256.

Zhelev, D., and D. Needham. 1994. The influence of electric fields on biological and model membranes. *In* Biological Effects of Electric and Magnetic Fields. Sources and Mechanisms. D. Carpenter and S. Ayrapetyan, editors. Academic Press, San Diego, CA. 105–142.

Zheng, Q., and D. C. Chang. 1991. High-efficiency gene transfection by in situ electroporation of cultured cells. *Biochim. Biophys. Acta.* 1088: 104–110.